molecules

MDPI

Article

The Potential Neuroprotective Effect of Thymoquinone on Scopolamine-Induced In Vivo Alzheimer's Disease-like Condition: Mechanistic Insights

Hend E. Abo Mansour [1,*], Aya Ibrahim Elberri [2], Mai El-Sayed Ghoneim [3], Waad A. Samman [4], Aisha A. Alhaddad [4], Mahmoud S. Abdallah [5], Eman I. El-Berri [6], Mohamed A. Salem [7] and Esraa M. Mosalam [1]

1 Biochemistry Department, Faculty of Pharmacy, Menoufia University, Shibin El-Kom 32511, Egypt; esraa.mosalam@phrm.menofia.edu.eg
2 Genetic Engineering and Molecular Biology Division, Department of Zoology, Faculty of Science, Menoufia University, Shibin El-Kom 32511, Egypt; ayaelbery62@science.menofia.edu.eg
3 Department of Pharmacology and Toxicology, Faculty of Pharmacy, University of Sadat City (USC), Sadat City 32897, Egypt; mai.ghoneim@fop.usc.edu.eg
4 Department of Pharmacology and Toxicology, College of Pharmacy, Taibah University, Medina 42353, Saudi Arabia; wsamman@taibahu.edu.sa (W.A.S.); aahaddad@taibahu.edu.sa (A.A.A.)
5 Clinical Pharmacy Department, Faculty of Pharmacy, University of Sadat City (USC), Sadat City 32897, Egypt; mahmoud.samy@fop.usc.edu.eg
6 Clinical Pharmacy Department, Faculty of Pharmacy, Tanta University, Tanta 31527, Egypt; eman.elberri@pharm.tanta.edu.eg
7 Department of Pharmacognosy, Faculty of Pharmacy, Menoufia University, Shibin El-Kom 32511, Egypt; mohamed.salem@phrm.menofia.edu.eg
* Correspondence: hend_elsaid@phrm.menofia.edu.eg; Tel.: +20-109-850-5161

Citation: Abo Mansour, H.E.; Elberri, A.I.; Ghoneim, M.E.-S.; Samman, W.A.; Alhaddad, A.A.; Abdallah, M.S.; El-Berri, E.I.; Salem, M.A.; Mosalam, E.M. The Potential Neuroprotective Effect of Thymoquinone on Scopolamine-Induced In Vivo Alzheimer's Disease-like Condition: Mechanistic Insights. *Molecules* **2023**, *28*, 6566. https://doi.org/10.3390/molecules28186566

Academic Editors: Maja Jazvinšćak Jembrek and Suzana Šegota

Received: 20 July 2023
Revised: 31 August 2023
Accepted: 5 September 2023
Published: 11 September 2023

Abstract: Background: Alzheimer's disease (AD) is a common neurodegenerative disorder without effective treatment. Thymoquinone (TQ) has demonstrated potential in exhibiting anti-inflammatory, anti-cancer, and antioxidant characteristics. Despite TQ's neuroprotection effect, there is a scarcity of information regarding its application in AD research, and its molecular trajectories remain ambiguous. Thus, the objective of the current investigation was to examine the potential beneficial effects and underlying mechanisms of TQ in scopolamine (SCOP)-induced neuronal injury to mimic AD in vivo model. Methods: Thirty mice were divided into normal, SCOP, and TQ groups. The Y-maze and pole climbing tests were performed to measure memory and motor performance. Afterwards, histopathological and immunohistochemical examinations were carried out. Furthermore, peroxisome proliferator-activated receptor gamma (PPAR-γ) signaling pathway-related proteins and genes were detected with an emphasis on the role of miR-9. Results: TQ has the potential to ameliorate cognitive deficits observed in SCOP-induced AD-like model, as evidenced by the improvement in behavioral outcomes, histopathological changes, modulation of the expression pattern of PPAR-γ downstream targets with a significant decrease in the deposition of amyloid beta (Aβ). Conclusions: TQ provided meaningful multilevel neuroprotection through its anti-inflammatory and its PPAR-γ agonist activity. Consequently, TQ may possess a potential beneficial role against AD development.

Keywords: Alzheimer's disease; scopolamine; thymoquinone; PPAR-γ; NF-κB; miR-9

1. Introduction

Alzheimer's disease (AD) is a neurological disorder that causes memory loss and other cognitive difficulties [1]. According to research by Brookmeyer et al. (2007), this type of dementia is common among the elderly and has a high mortality rate [2]. The health burden associated with AD is tremendous, and it is anticipated to increase substantially by 2050 [3].

The etiology of AD remains unclear; however, two prominent pathological features are observed: the presence of senile plaques and the deposition of neurofibrillary tangles. The

neurotoxic senile plaques are composed of amyloid beta (Aβ) peptide resulting from the proteolytic cleavage of amyloid precursor protein (APP) by β-site amyloid precursor protein cleaving enzyme-1 (BACE-1), w hereas the neurofibrillary tangles are composed of aberrant tau protein filaments [4,5]. Consequently, this triggers a cascade of events that culminate in neurodegeneration, oxidative stress, synaptic dysfunction, and neuroinflammation [1,6]. Furthermore, decreased acetylcholine and glutamatergic deficits play a crucial part in the etiology of AD [4]. For this reason, N-methyl-D-aspartic acid receptor antagonists and acetylcholinesterase inhibitors have been validated as AD therapy [7,8]. The drawbacks of the currently available treatments and poor therapeutic efficacy have driven the researchers to develop novel approaches [9]. It is, therefore, worthwhile to investigate the efficacy of possible neuroprotective agents for AD [10].

MicroRNAs (miRNAs) have been recognized as a promising subject for exploring the pathophysiology of AD [11]. Mounting data have revealed that many circulating miRNAs, including miR-29, miR-146, and miR-9, are implicated in the Aβ-induced pathogenesis of AD [12–14]. Multiple research groups have shown that depletion of miR-9 is potentially connected with the progression of AD [15–17], and its overexpression ameliorates Aβ1–42-induced synaptotoxicity [18]. The findings supported the hypothesis that miR-9 could be intricately linked to the amelioration of AD. Thus, it can be inferred that miR-9 could potentially serve as a crucial modulator of AD.

Other signaling pathways have also been concerned in the pathogenesis of AD. The nuclear factor kappa B (NF-κB) transcription factor has been implicated as a risk factor for neurodegeneration and the advancement of AD [19,20]. Upon stimulation, inhibitory kappa B kinase (IKK) complex phosphorylates Inhibitory kappa B subunit alpha (IκB-α) and initiates its degradation in the proteasome, resulting in a rapid nuclear transport of NF-κβ protein [21,22]. NF-κB-induced activation further led to the upregulation of AβPP/BACE1 expression, resulting in Aβ accumulation [23]. Moreover, peroxisome proliferator-activated receptor gamma (PPAR-γ) has been shown to inhibit Aβ and tau accumulation, lessen neuroinflammation, and enhance memory [24].

Natural substances have captured much more attention owing to their content of many biologically active compounds [25–27]. Thymoquinone (TQ), the primary bioactive constituent of the volatile oil extracted from Nigella sativa seeds, has been studied extensively for its diverse range of biological properties [28,29]. Numerous investigations shed light on the neuroprotective effect of TQ on mitigating the progression of AD symptoms by inhibiting NF-κB activation [30–32]. Nevertheless, the precise molecular mechanisms underlying these benefits remain poorly comprehended.

Scopolamine (SCOP) is a competitive, nonselective muscarinic acetylcholine receptor antagonist that is frequently used to cause cognition and memory deficits in animal models by blocking cholinergic neurotransmission [33]. This pattern of memory dysfunction is similar to that in patients who suffer from AD [34].

Consequently, the present study endeavors to experimentally induce an AD-like model via SCOP in mice and to examine the ability of TQ to enhance cognitive impairment and restoration of synaptic proteins through its PPAR-γ agonist activity with a particular focus on miR-9, which may lead to decreased deposition of amyloid β, the major hallmark of AD.

2. Results

2.1. Behavioral Performance

Figure 1a shows the results of the Y-maze behavioral test. There was a significant decline (↓ 51.65%, $p < 0.001$) in the cumulative percent of spontaneous alteration (% SA) of the total of seven days in the SCOP group compared to the normal control. Pretreatment with TQ increased the cumulative % SA by 22.88% relative to SCOP but it was non-statistically significant ($p = 0.219$). Regarding the performance of the mice in the pole climbing test, the SCOP group exhibited significant increase in the cumulative time required to reach the ground (↑ 81.93%, $p < 0.001$) compared to normal mice. TQ-pretreated mice

showed significant less cumulative time (↓ 40.84, $p = 0.035$) to reach the base relatively to the SCOP group (Figure 1b).

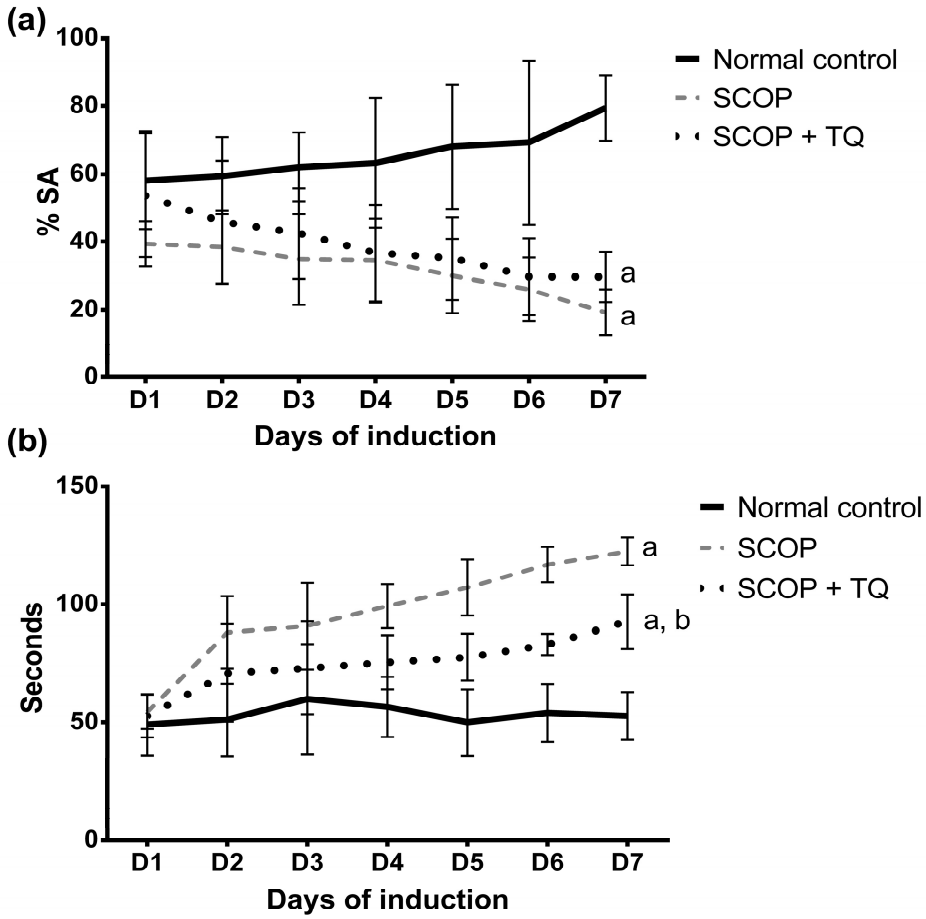

Figure 1. Effect on behavioral tests. (**a**) Y-maze test and (**b**) Pole climbing test. Data are presented as the mean ± SD, n = 10, and were analyzed using one-way ANOVA followed by Tukey post hoc test, $p < 0.05$. a: significant versus normal control and b: significant versus SCOP group. SCOP: scopolamine, TQ: thymoquinone, SA%: percent of spontaneous alteration.

2.2. Histopathological Examination

Figure 2 shows a photomicrograph of a section of the cerebral cortex (a1) of a normal control mouse showing normal pyramidal cells and granular cells (arrow) with some astrocytes (red arrow head). The CA1 (a2) and CA3 (a3) regions showed molecular layer (M), pyramidal layer (P), and polymorphic layer (PL). The pyramidal layer of CA1 expressed 4-5 compact layers of small pyramidal cells (arrow) most with vesicular nuclei, whereas that of CA3 region expressed few layers of large pyramidal cells (arrow) also with vesicular nuclei and some astrocytes (red arrow head). The dentate gyrus area (a4) showed molecular layer (M), granular layer (G), and astrocytes (red arrow head). The hematoxylin and eosin (H & E) staining of cerebral cortex (b1) of a SCOP mouse revealed some irregular darkly stained pyramidal cells with pyknotic nuclei and surrounded by haloes (arrows). Other pyramidal cells appeared with faintly stained cytoplasm and nuclei (curved arrow). There were also dilated congested blood vessels (BV) with inflammatory cells in it (C), multinuclear giant cells (star), and extensive neuropil vacuolization (square). The CA1 area (b2) showed numerous degenerated neurons (arrows) and many vacuolation, whereas the CA3 area (b3) revealed also numerous degenerated neurons (arrows) and large congested blood vessel (BV). There were darkly stained nuclei (arrows) and vacuolated cytoplasm (V) in the dentate gyrus region (b4). TQ-pretreated group showed normal pyramidal cells and granular cells (arrow), but there were some congested blood vessels (BV) in the cerebral

cortex (c1). The CA1 area (c2) expressed molecular layer (M), pyramidal layer (P), and polymorphic layer (PL), but there were cells with pyknotic nuclei (arow) and also some congested blood vessels (BV). The CA3 area (c3) showed slight improvement compared to SCOP only group, but there were cells with pyknotic nuclei (arow) and some congested blood vessels (BV). The dentate gyrus region (c4) revealed molecular layer (M), granular layer (G), and multiple congested blood vessels (BV). Regarding the quantification of the pyramidal cells, the SCOP group showed significant decrease ($p < 0.001$) by 56.29% compared to the normal control. The TQ-pretreatment significantly ($p < 0.001$) increased the number of the cells by 85.6% compared to the SCOP group as presented in Figure 2.

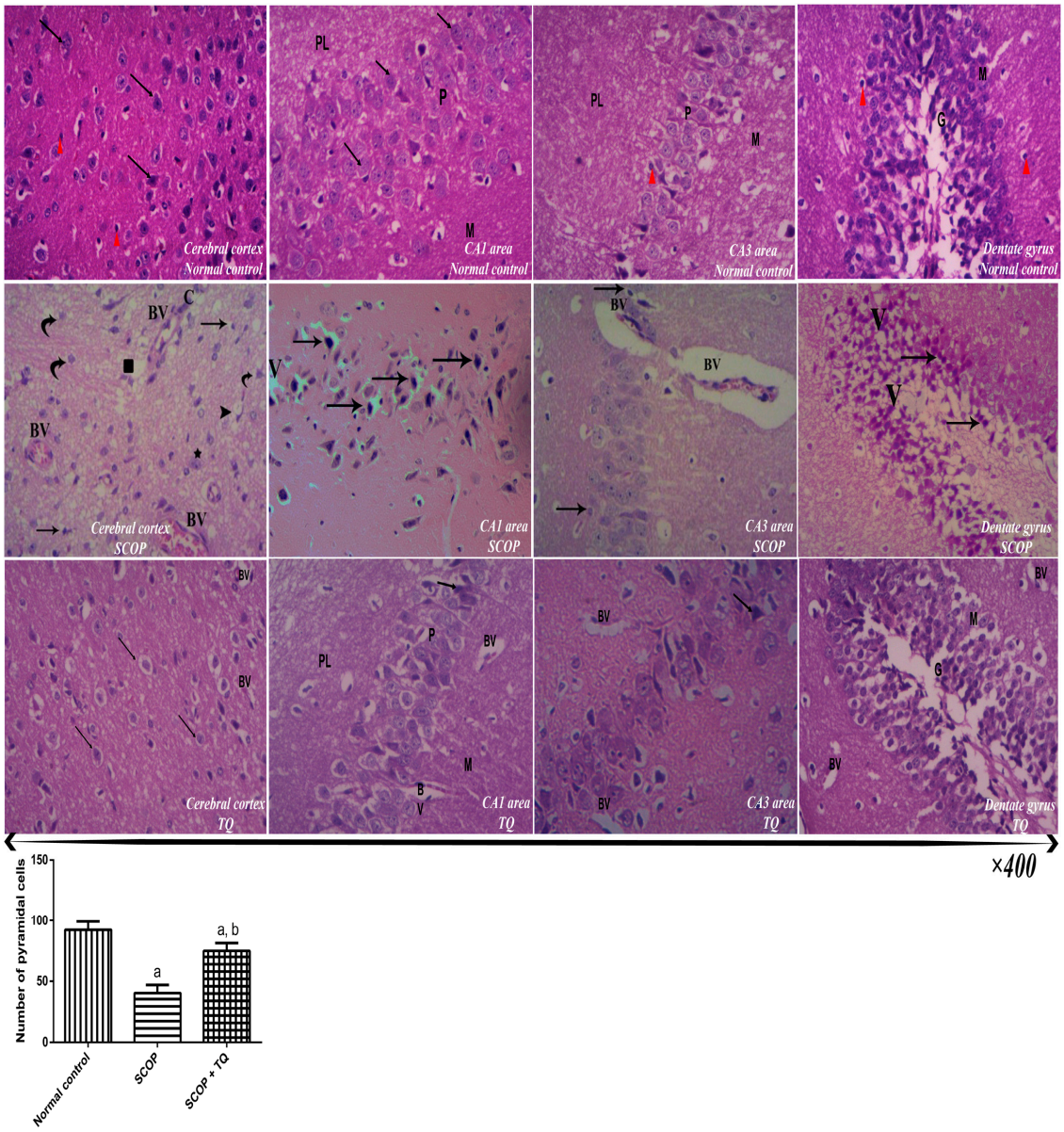

Figure 2. Effect on histopathological examination by hematoxylin and eosin stain and its morphometric analysis. Four different brain regions were examined: 1: cerebral cortex, 2: CA1 area, 3: CA3 area, and 4: dentate gyrus area. Data are presented as the mean ± SD, n = 10, and were analyzed using one-way ANOVA followed by Tukey post hoc test, $p < 0.05$. a: significant versus normal control and b: significant versus SCOP group. SCOP: scopolamine, TQ: thymoquinone, PL: polymorphic layer, P: pyramidal layer, M: molecular layer, G: granular layer, BV: blood vessel, C: inflammatory cells, V: vacuolated cytoplasm, Red arrow head: astrocytes.

Figure 3 shows staining of the brain tissue with Congo red. Staining of the brain tissue of a normal mouse showed normal cerebral cortex (a1), normal CA1 (a2), normal CA3 (a3), and normal dentate gyrus (a4) with no detectable microscopic abnormalities. Photomicrographs of the same examined brain regions of SCOP mouse showed multiple congophilic amyloid plaques (White arrow). TQ-pretreated mouse revealed minimal amyloid deposition in all examined brain areas. The morphometric analysis showed significant ($p < 0.001$) drop in the count of amyloid plaques in the TQ-pretreated group by 77.99% compared to the SCOP group as displayed in Figure 3.

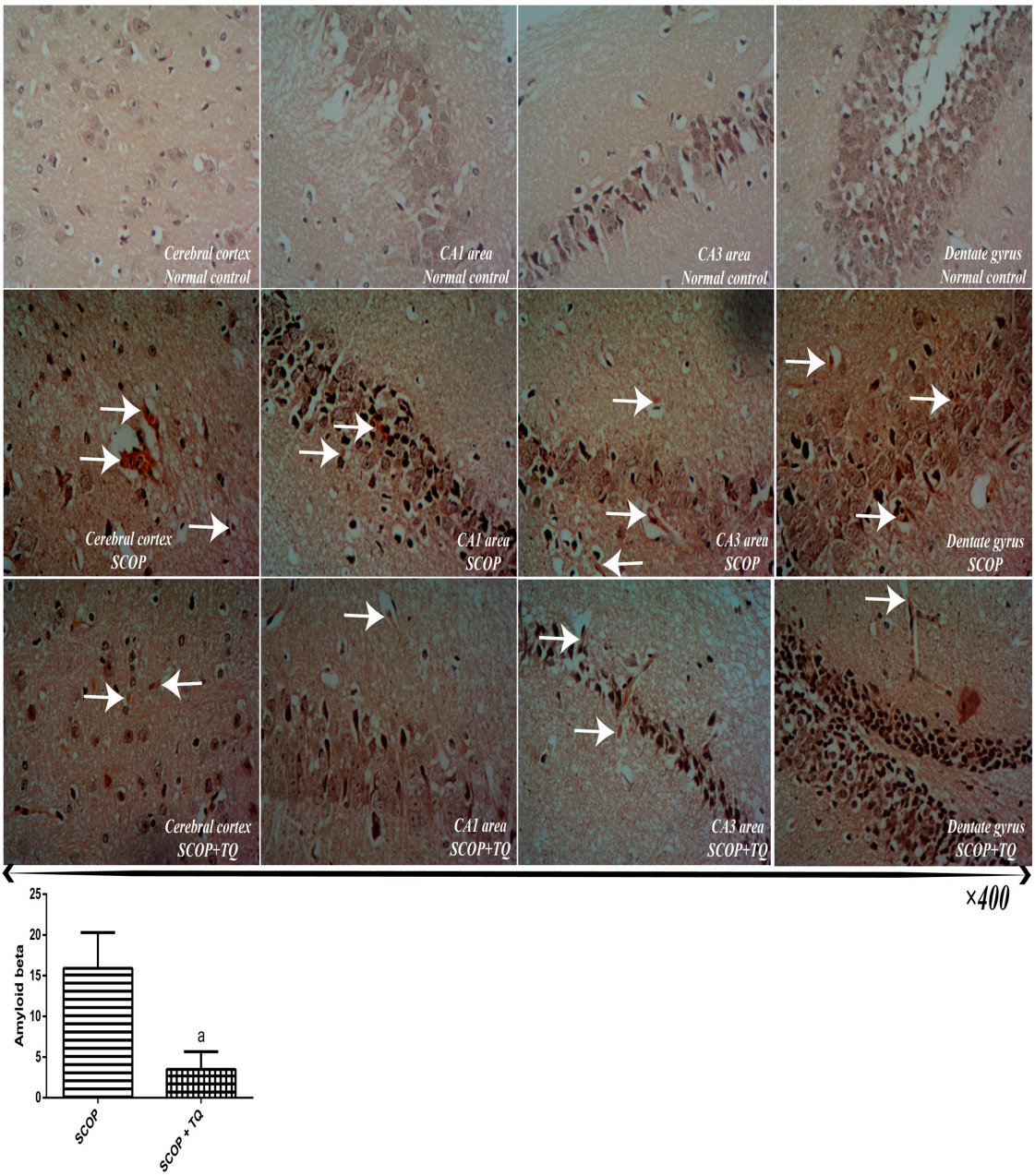

Figure 3. Effect on histopathological examination by Congo red staining and its morphometric analysis. Four different brain regions were examined: 1: cerebral cortex, 2: CA1 area, 3: CA3 area, and 4: dentate gyrus area. Data are presented as the mean ± SD, n = 10, and were analyzed using one-way ANOVA followed by Tukey post hoc test, $p < 0.05$. a: significant versus SCOP group. SCOP: scopolamine, TQ: thymoquinone, White arrow: Amyloid plaques deposition.

2.3. Immunohistochemical Examination

Figure 4 represents the immune-staining of NF-κB. All examined regions of the brain of the normal control showed negligible expression of NF-κB (a1, a2, a3, and a4). In contrast, the photomicrograghs of SCOP control group revealed severe expression of NF-κB (b1, b2, b3, and b4) (Black arrow). Pre-treatment with TQ showed minimal reaction toward NF-κB antibody (c1, c2, c3, and c4). The quantitative measurement showed that SCOP significantly ($p < 0.001$) increased NF-κB by 12.04 folds compared to the normal control. In contrast, pretreatment of the mice with TQ significantly ($p < 0.001$) lowered NF-κB by 62.68% relatively to the disease control group (Figure 4).

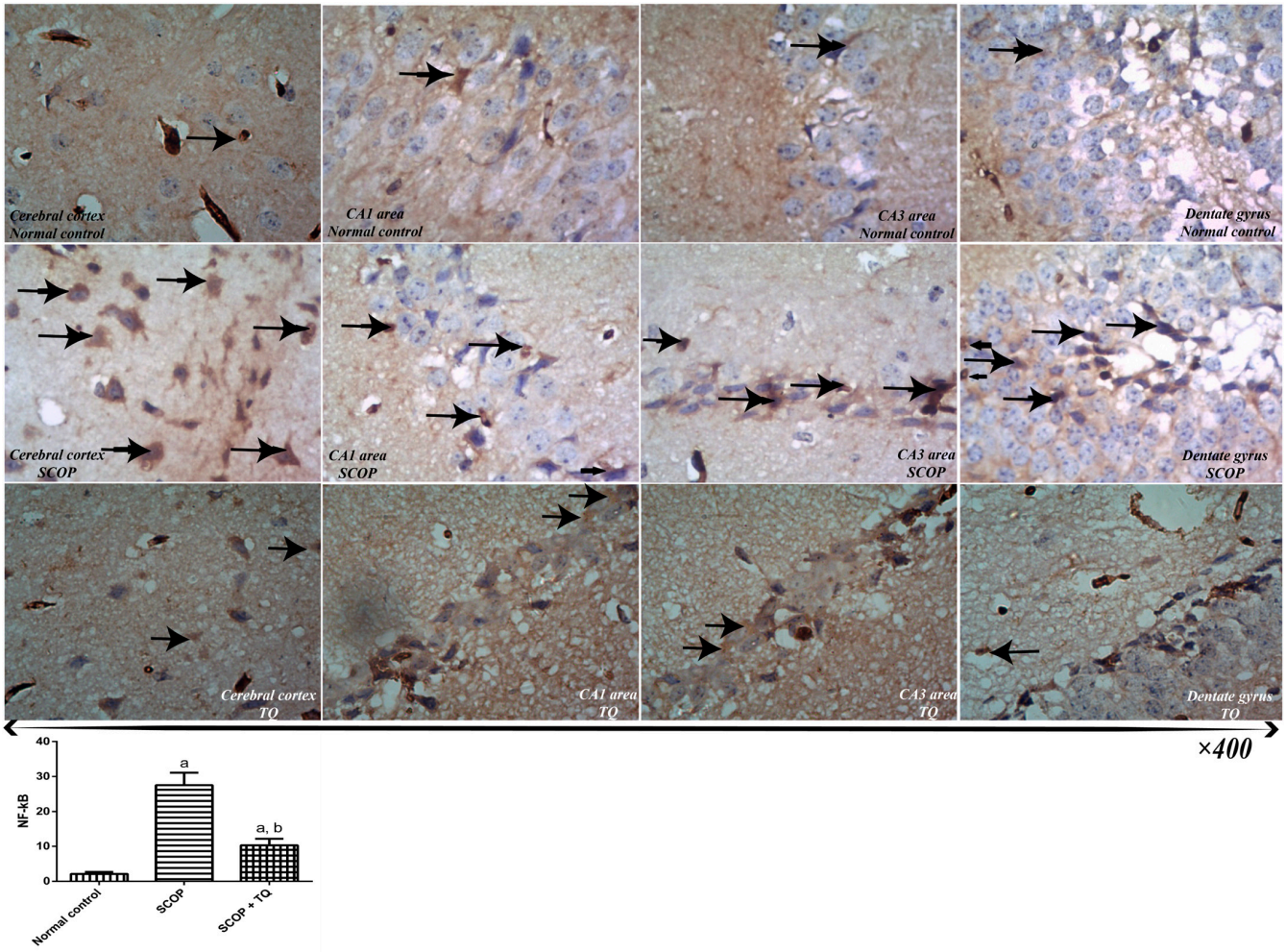

Figure 4. Effect on immunohistochemistry for NF-κB and its morphometric analysis. Four different brain regions were examined: 1: cerebral cortex, 2: CA1 area, 3: CA3 area, and 4: dentate gyrus area. Data are presented as the mean ± SD, n = 10, and were analyzed using one-way ANOVA followed by Tukey post hoc test, $p < 0.05$. a: significant versus normal control group and b: significant versus SCOP group. SCOP: scopolamine, TQ: thymoquinone, NF-κB: nuclear factor kappa-light-chain-enhancer of activated B cells. Black arrow: NF-κB expression.

Regarding the immunostaining of phosphorylated tau protein (Ptau), photomicrographs of the control group showed very mild deposition of the precipitated protein. The SCOP group exhibited sever reaction toward the added antibody, which reflect highly deposited amount of Ptau protein (Red arrow). Pre-treatment with TQ showed moderate expression of Ptau. In a quantitative term, the SCOP group significantly ($p < 0.001$) elevated Ptau by 38 fold compared to normal, whereas TQ significantly ($p < 0.001$) decreased Ptau by 58.33% relatively to the disease control group as shown in Figure 5.

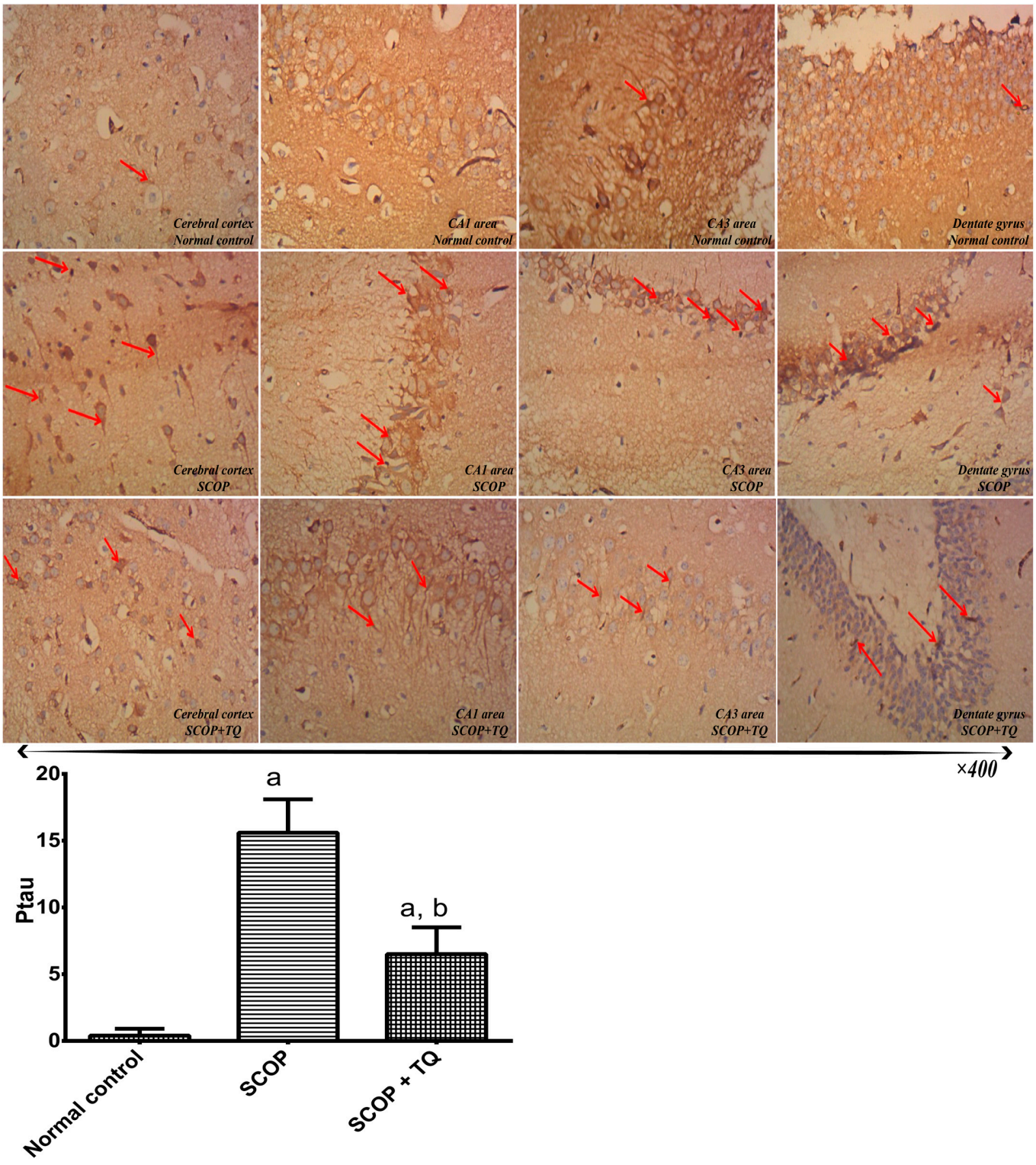

Figure 5. Effect on immunohistochemistry for Ptau and its morphometric analysis. Four different brain regions were examined: 1: cerebral cortex, 2: CA1 area, 3: CA3 area, and 4: dentate gyrus area. Data are presented as the mean ± SD, n = 10, and were analyzed using one-way ANOVA followed by Tukey post hoc test, $p < 0.05$. a: significant versus normal control group and b: significant versus SCOP group. SCOP: scopolamine, TQ: thymoquinone, Ptau: phosphorylated tau protein. Red arrow: Ptau deposition.

2.4. Effect on Mitochondrial Membrane Potential

Figure 6 shows staining of cellular mitochondria in the studied groups. Normal control group was effectively stained with tetramethylrhodamine, methyl ester (TMRM) and gave multiple green fluorescent spots, indicating massive number of lived intact mitochondria. In contrast, SCOP-treated group exhibited minimal fluorescence signals. Pretreatment with TQ restored the mitochondrial membrane potential (MMP) and showed reasonable fluorescent spots. In terms of CTCF, the SCOP group significantly ($p < 0.001$) decreased CTCF by 77.01% compared to the normal control, whereas TQ-pretreatment significantly ($p = 0.047$) increased CTCF by 69.57% compared to SCOP only group.

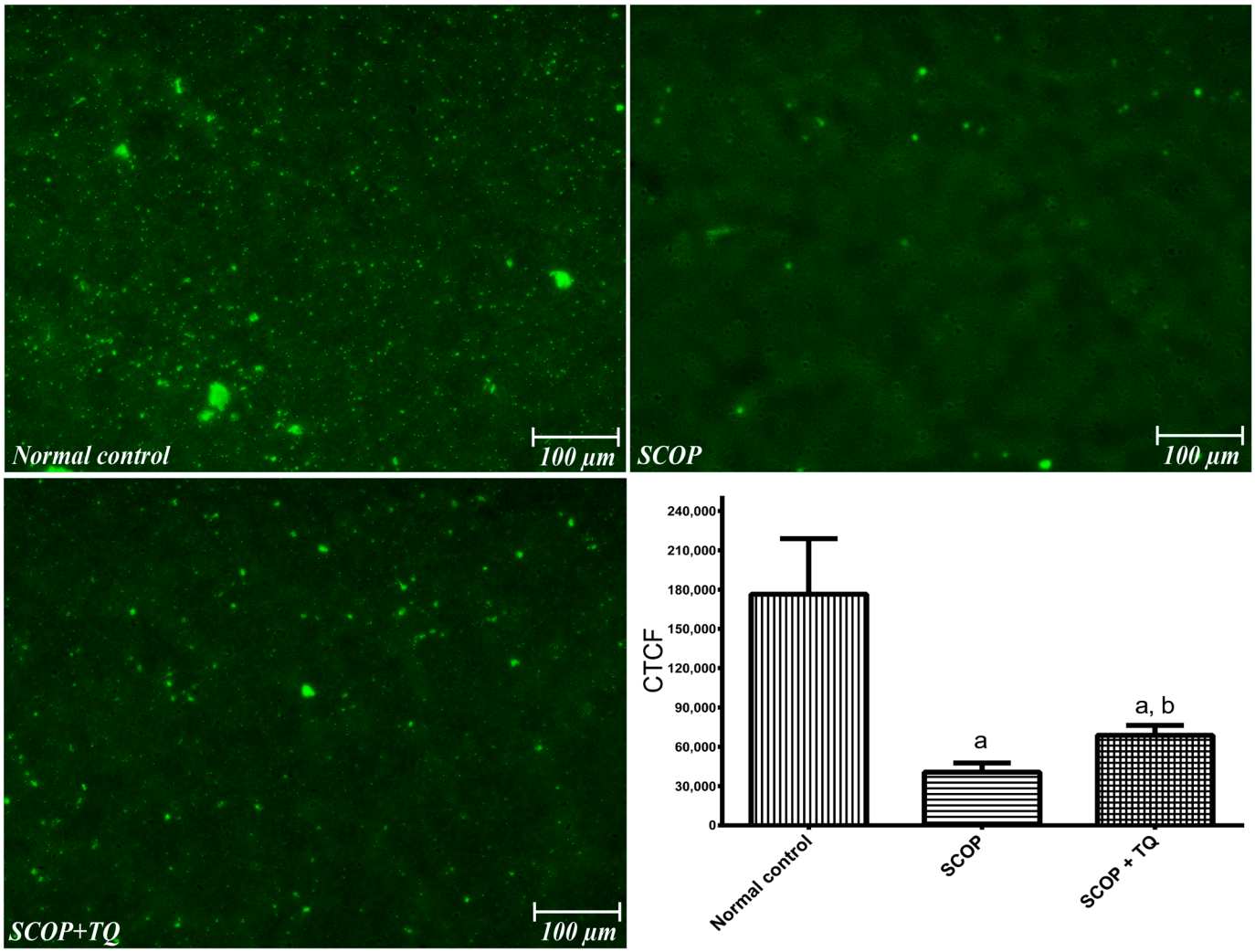

Figure 6. Effect on mitochondrial membrane potential and its quantitative measurement by CTCF. Data are presented as the mean ± SD, n = 10, and were analyzed using one-way ANOVA followed by Tukey post hoc test, $p < 0.05$. a: significant versus normal control group and b: significant versus SCOP group. SCOP: scopolamine, TQ: thymoquinone, CTCF: corrected total cell fluorescence, green spots: Lived intact mitochondria.

2.5. Effect on Inflammatory Cytokines

Induction of the disease by SCOP significantly ($p < 0.001$) increased the serum level of TNF-α and IL-6 by 4.18 and by 1.76 fold, respectively, compared to the normal control. Pretreatment with TQ significantly ($p < 0.001$) decreased the serum level of the cytokines by 38.99 and by 33.76%, respectively, in comparison with the SCOP group as presented in Table 1.

Table 1. Effect of TQ on inflammatory cytokines.

	Normal Control	SCOP	SCOP + TQ
TNF-α (pg/mL)	29.857 ± 3.913	154.928 ± 12.789 [a]	94.517 ± 5.287 [a,b]
IL-6 (pg/mL)	27.8 ± 6.142	77 ± 5.597 [a]	51 ± 5.83 [a,b]

Data are presented as the mean ± SD, n = 10, and were analyzed using one-way ANOVA followed by Tukey post hoc test, $p < 0.05$. [a]: significant versus normal control group and [b]: significant versus SCOP group. SCOP: scopolamine, TQ: thymoquinone, TNF-α: tumor necrosis factor-alpha, IL-6: interleukin 6.

2.6. Effect on IκB-α and IKK-α

The SCOP group exhibited significant ($p < 0.001$) decrease in the concentration of IκB-α by 69.35% with a significant ($p < 0.001$) increase by 3.57 fold in the concentration of IKK-α versus the normal control. In contrast, pretreatment with TQ has reversed the concentration of these proteins by 1.08 fold for IκB-α and by 13.7% for IKK-α ($p < 0.001$ and $p = 0.118$, respectively vs. SCOP group) as presented in Figure 7.

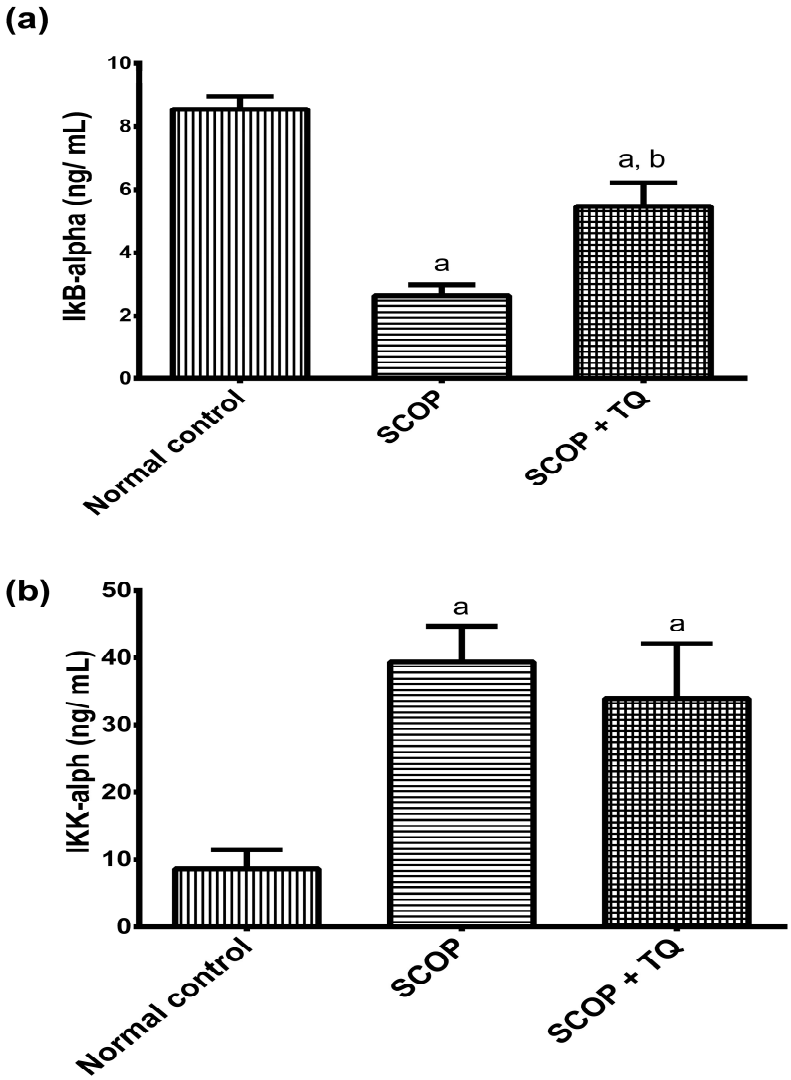

Figure 7. Effect on the brain content of IκB-α and IKK-α. (**a**) IκB-α and (**b**) IKK-α. Data are presented as the mean ± SD, n = 10, and were analyzed using one-way ANOVA followed by Tukey post hoc test, $p < 0.05$. a: significant versus normal control group and b: significant versus SCOP group. SCOP: scopolamine, TQ: thymoquinone, IκB-α: Inhibitory kappa B subunit alpha, IKK-α: inhibitory kappa B kinase subunit alpha.

2.7. Effect on miR-9, PPAR-γ, NF-κB, BACE-1, and Synapsin-2

Figure 8 shows that the SCOP group significantly downregulated PPAR-γ, synapsin-2, and miR-9 (66.28, 80.06, and 85.15%, respectively, $p < 0.001$) with a significant upregulation for NF-κB, and BACE-1 (13.37 and 4.37 folds, respectively, $p < 0.001$) compared to the normal control group. Relatively to the SCOP group, pretreatment with TQ showed a significant upregulation for PPAR-γ, synapsin-2, and miR-9 (1.09, $p = 0.005$; 2.06, $p = 0.001$; and 2.19, $p = 0.016$ folds, respectively) with a significant downregulation for NF-κB and BACE-1 (65.43 and 42.59%, $p < 0.001$, respectively).

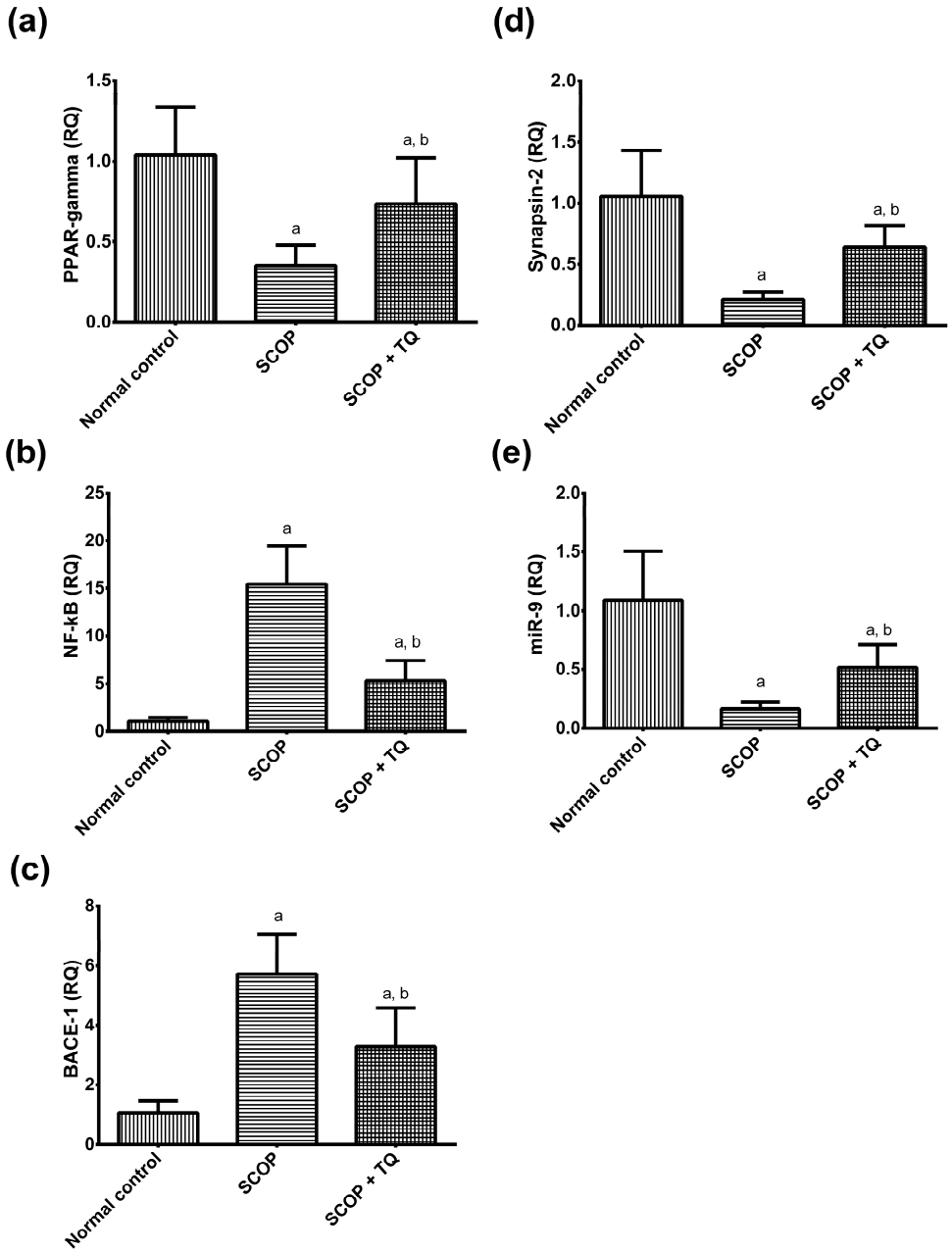

Figure 8. Effect on the brain content of (**a**) PPAR-γ, (**b**) NF-κB, (**c**) BACE-1, (**d**) synapsin-2, and (**e**) miR-9. Data are presented as the mean ± SD, n = 10, and were analyzed using one-way ANOVA followed by Tukey post hoc test, $p < 0.05$. a: significant versus normal control group and b: significant versus SCOP group. SCOP: scopolamine, TQ: thymoquinone, PPAR-γ: peroxisome proliferator-activated receptor gamma, NF-κB: nuclear factor kappa-light-chain-enhancer of activated B cells, BACE-1: β-site amyloid precursor protein cleaving enzyme 1.

2.8. Effect on Amyloid Beta

SCOP has significantly elevated the amyloid content in the brain of the disease control group (44.37 folds vs. normal $p < 0.001$). On the other hand, protection of the mice with TQ has significantly lowered the concentration of $A\beta_{1–42}$ by 47.1% relatively to the SCOP only ($p < 0.001$) as shown in Figure 9.

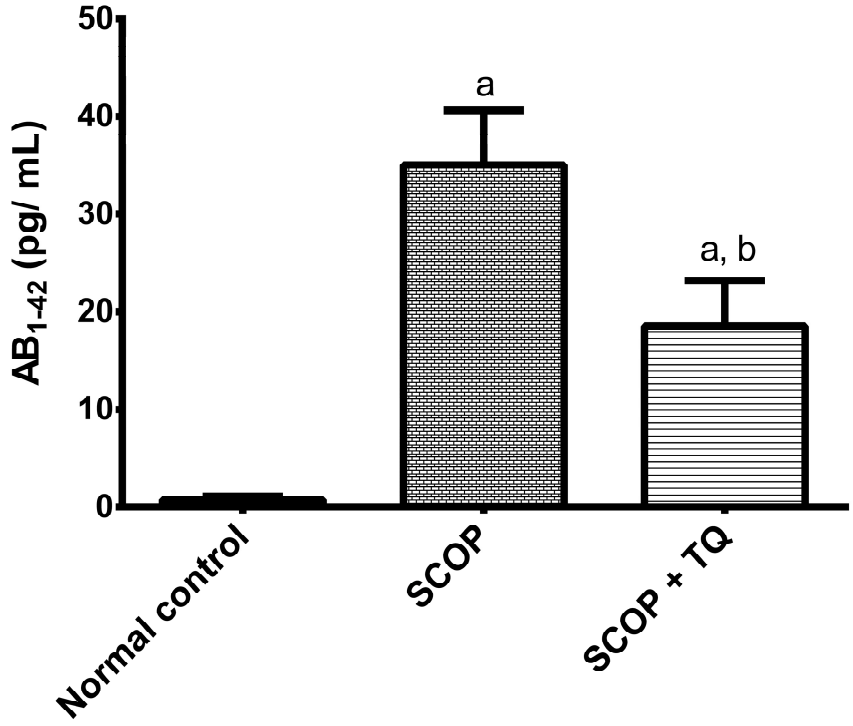

Figure 9. Effect on the brain content of amyloid beta. Data are presented as the mean ± SD, n = 10, and were analyzed using one-way ANOVA followed by Tukey post hoc test, $p < 0.05$. a: significant versus normal control group and b: significant versus SCOP group. SCOP: scopolamine, TQ: thymoquinone, $A\beta_{1–42}$: amyloid beta sequence 1–42.

3. Discussion

To the best of our knowledge, the current study provides evidence of the impact of TQ therapy on SCOP-triggered neurodegeneration in mice, with a particular focus on its modulatory effect on the PPAR-γ signaling pathway. The findings of the current investigation indicated that SCOP-induced cognitive impairment led to distortion of histopathological findings and the deposition of amyloid plaques in various brain regions. These findings were consistent with a general decline in the percentage of spontaneous alternations and an increase in cumulative time in pole climbing behavioral tests, which were in line with other recent studies [35,36], indicating the cognitive impairment of SCOP in rats. On the other hand, the administration of TQ resulted in a notable enhancement of the aberrant histopathological alterations and a rise in the count of pyramidal cells. Additionally, it successfully counteracted the cognitive impairment and motor deficiencies induced by SCOP, as documented by Poorgholam et al. (2018), who elucidated that TQ ameliorated learning functioning and memory loss in a rat model of AD [37].

A plethora of studies has indicated that the activation of PPAR-γ-dependent mechanism can improve cognitive deficits and reduce Aβ deposition in AD [38,39]. Intriguingly, the activation of PPAR-γ was found to inhibit several transcription factors that play a role in inflammation, including NF-κB [40]. Consequently, the activation of PPAR-γ leads to reduction in inflammation by suppressing NF-κB [41]. In addition, Dehmer et al. (2004) reported that the administration of PPAR-γ agonists leads to downregulation of IKK-α with concomitant increase in the level of IκB-α and a decrease in the nuclear translocation

of NF-κB [42]. Alternatively, it has been reported that PPAR-γ modulated APP processing through the negative regulation of BACE-1 expression and promoted Aβ clearance [38,43].

Additionally, Xiang et al. (2012) has documented that SCOP reduced PPAR-γ activity leading to memory impairment, which was reversed by the effect of PPAR-γ agonist [44]. Furthermore, treatment with PPAR-γ agonist can lead to a reduction in the deposited Ptau protein [45]. In line with this notion, our experimental model revealed a conspicuous downregulation in PPAR-γ gene expression with significant elevated level of Aβ and Ptau, the two hallmarks of AD. Nonetheless, pretreatment with TQ, a PPAR-γ agonist, counteracted the effect of SCOP, which could explain its beneficial role against SCOP-induced neuronal injury and cognitive impairment. In line with our findings, according to Chen et al. (2018), TQ-induced activation of PPAR-γ has been found to decrease spinal cord injury [46]. Moreover, a contemporary study has reported that TQ enhanced the cognitive deficits caused by ischemic stroke via activation of PPAR-γ [47]. Another study reported the neuroprotective effect of TQ also through reducing the level of Ptau in aluminum chloride-induced AD-like model [48]. These findings highlighted a novel molecular path where TQ ameliorated memory problems in AD through upregulation of PPAR-γ.

NF-κB is a transcriptional protein that is activated by various factors associated with AD pathogenesis [20]. The activation of NF-κB is contingent upon the phosphorylation by IKK-α, which leads to the degradation of inhibitory protein IκBα and the consequent translocation of NF-κB to the nucleus [21]. This transcription factor is responsible for regulating the expression of various inflammatory cytokines, such as TNF-α and IL-6 [49]. Furthermore, the activation of NF-κB signaling pathway stimulates the expression of BACE-1, generation of proinflammatory cytokines, and deposition of Aβ, leading to a detrimental cycle of neuroinflammation [20].

The outcomes of our study exhibited a significant inhibition of NF-κB, which was augmented by SCOP administration. Concurrently, the SCOP administration elicited a significant elevation in the concentration of IKK-α, while suppressing the level of lκB-α. On the contrary, TQ-pretreated mice demonstrated a reversal in the levels of the defined proteins. Consistent with these results, our study has indicated a notable increase in the concentrations of the proinflammatory cytokines, TNFα and IL6, among the SCOP cohort. Nevertheless, the TQ intervention succeeded in minimizing the concentrations of these cytokines. Consistent with our findings, it was elucidated that TQ could impede neuroinflammation triggered by SCOP and subsequently repressed proinflammatory mediators through regulation of the PI3K/Akt/NF-κB signaling hub [50], and modulation of Toll-like receptors [51]. More importantly, TQ exhibited inhibitory effects on osteoclastogenesis via reduction in phosphorylation of IKKα/β, thereby suppressing the activation of NF-κB [52]. Taken altogether, this is the primary attempt that illustrates the inhibitory effect of TQ on the activation of NF-κB and the alleviation of consequent mechanism-induced neuronal degeneration through the activation of PPAR-γ.

Mitochondrial impairment is widely recognized as a significant contributor to the pathogenesis of AD [53]. A growing body of evidence suggested that dysregulation of MMP may occur due to oxidative stress and neuroinflammation [53,54]. Furthermore, the process of excessive phosphorylation of tau protein has been observed to impede mitochondrial transport at the synapse, causing severe oxidative stress [55]. Surprisingly, PPAR-γ agonist may play a role in regulating mitochondria and mitigating its dysregulation in AD, as elucidated by previous study [56]. Our findings have indicated that the MMP was disrupted following the administration of SCOP, which is consistent with preceding studies [57–59], indicating the cognitive impairment due to oxidative stress induced by SCOP. However, TQ administration resulted in the prevention of mitochondrial dysfunction and the restoration of MMP. The findings of our study are consistent with recent investigations indicating that TQ may possess neuroprotective properties hampering the mitochondrial membrane depolarization, ROS generation, and Aβ deposition in neurotoxicity model [30,60].

MicroRNAs are widely recognized as a significant factor that affects cognitive performance by disrupting genes crucial to the progression of AD. Interestingly, miR-9 has

been identified as a critical regulator of BACE-1 enzyme, which plays a vital role in the accumulation of Aβ [11]. Additionally, a study conducted by Hébert, et al. found that the increase in BACE-1/beta secretase expression in AD is linked to the depletion of miR-9 [12]. More importantly, miR-9 has been documented to impede the NF-κB signaling trajectory in different models [61–63]. To the best of our knowledge, this study is the first to elucidate the effect of TQ on miR-9 in SCOP-induced neurodegeneration. In the present study, after administration of SCOP, a significant reduction in the miR-9 gene expression was observed, which was significantly reversed by TQ pretreatment. Our results are in harmony with other studies elucidating the correlation between the reduction in miR-9 and the inhibition of neuroinflammation [14,64,65]. Furthermore, it has been reported that the upregulation miR-9 expression led to improvement in learning and memory capabilities, lessening Aβ aggregation, and tau accumulation [66,67].

BACE-1 is the primary enzyme responsible for the initiation of Aβ accumulation, and its inhibition is considered a key strategy to impede the progression of AD [68,69]. Mechanistically, the activation of PPAR-γ leads to the suppression of BACE-1 gene expression and inhibition of Aβ production [70,71]. These findings suggested that PPAR-γ plays a regulatory role in the functioning of BACE-1, and its activation can effectively impede the activity of BACE-1. In the current study, administration of SCOP increased the level of BACE-1, going in the same direction with other a recent study [72]. Nevertheless, the pretreatment by TQ exhibited a counteractive impact on the influence of SCOP. This conclusion aligns with prior studies that showed the neuroprotective properties of TQ via downregulation of BACE-1 in various models of AD [73,74]. This, in turn, provides additional evidence that TQ hindered accumulation of Aβ by controlling the expression of BACE-1 via PPAR-γ-dependent mechanism.

It is well known that the inhibition of synapsin-2 is linked to intricate memory impairment, disruption of the synaptogenesis process, and aggregation of Aβ [75], which can be attributed to the NF-κB activation [76]. Intriguingly, Li et al. (2017) has established a correlation between synaptic proteins and miR-9. In this context, Osthole exerts its neuroprotective effect by boosting the synaptic proteins levels, leading to elevation in miR-9 expression [66]. Furthermore, Chiang et al. (2014) have documented the advantageous impacts of PPAR-γ agonists in enhancing synaptic plasticity and preventing neuronal degeneration [77]. Our model has demonstrated a considerable reduction in synapsin-2 level, which is in harmony with Zhang et al. (2022) demonstrating memory impairment and synaptic damage in rats [78]. Conversely, our research represents the initial attempt that highlights the aptitude of TQ to elevate synapsin-2 concentration. The outcomes of this study validated the findings of a prior study, which demonstrated that ginsenoside enhanced cognitive function by increasing synapsin-2 expression in the hippocampus [79]. Additionally, Beker et al. (2018) has stated that TQ improves synaptic plasticity, thereby facilitating the proliferation of new neurons and enhancing neuronal viability [32].

Ultimately, TQ's ability to hinder neurodegeneration and cognitive decline reflects its capacity to upregulate synapsin-2 expression via the activation of the PPAR-γ signaling trajectory.

4. Materials and Methods

4.1. Animals

Adult male Albino mice were obtained from The Egyptian Organization for Biological Products and Vaccines (VACSERA, Cairo, Egypt). The mice were subjected to suitable laboratory conditions, including controlled temperature (25 ± 1 °C), relative humidity (55 ± 5%), and a 12 h light–dark cycle. The mice were also provided with a standard diet and tap water ad libitum and were acclimatized for about one month at the animal facility. The study protocol was approved by the Research Ethical Committee (Faculty of Science, Menoufia University, Shibin El-Kom, Egypt, FGE123) and it complies with the Guide for the Care and Use of Laboratory Animals (National Research Council).

4.2. Experimental Design

Thirty mice (n = 10) were randomly divided into three groups; mice in the 1st group were injected i.p. with normal saline and received corn oil orally (normal control group), mice in the 2nd group were injected with SCOP dissolved in normal saline at a dose of 0.5 mg/kg i.p. and received corn oil orally [80] for 7 consecutive days (SCOP group) starting from the eighth day until the fourteenth day, and the mice in 3rd group were received TQ dissolved in corn oil at a dose of 50 mg/kg/day intra-gastrically [81] starting from day one and continued for 14 days (SCOP + TQ group).

4.3. Behavioral Tests

The animals were transferred into the testing room at least 1 h before the commencement of behavioral tests in order to adapt. The testing room's temperature and humidity were similarly adjusted to those of a typical home. The behavioral tests were performed from the eighth day until the fourteenth day 30 min after SCOP injection. The day of SCOP induction was designated to be D1 and the end was at D7.

The Y-maze task is used to measure spontaneous alternation behavior and exploratory activity. The dimensions of the Y-shaped holding cage were 40 cm (length), 30 cm (height), and 15 cm (width). Each mouse was placed in one trial and allowed to freely discover the maze for 5–8 min. Subsequent inserts into the three arms on overlapping triplet sets constituted an alternating pattern. Alternations and the total number of switches were registered. The alternation, expressed as percentage, was determined by dividing the number of actual alternations by the number of possible alternations (defined as the total number of arm entries minus two) [53]. The motor function was also evaluated using a pole climbing procedure. Each mouse was placed at the top of a pole with uphill head position and the time taken by the mouse to correct his head down and descend to the floor was registered. The time of 120 s was clocked for mouse who dropped from the pole [53].

4.4. Sample Collection

At the end of the experiment, the mice were sacrificed under light halothane anesthesia and blood samples were collected in plain vacutainers to separate the serum for determination of inflammatory cytokine. The brain tissue was extracted, washed, and divided into parts. One part was kept in 10% buffered formalin for histopathological and immunohistochemical examination, whereas another part was immediately homogenized for visualization of mitochondria with a specific fluorescent dye. The other parts were maintained in −80 °C for further biochemical analyses.

4.5. Histopathological Examination

Part of the paraffin blocks was sectioned at 4–5 m and stained with Hematoxylin and Eosin (H&E) for visualization of pathological changes. Other blocks were stained with Congo red for visualization of Aβ [82]. The pathologist was evaluated the histological changes in four brain regions: cerebral cortex, CA1, CA3, and dentate gyrus using a light microscope at ×400 and ×200 magnification for H&E and Congo red, respectively. The morphometry was determined via a subjective counting of the number of the pyramidal cells for H&E saining and the number of Aβ for Congo red staining.

4.6. Immunohistochemical Examination

The paraffin blocks from the studied groups were sectioned and immunostained with anti-NF-κB P65 polyclonal antibody purchased from Elabscience® (Cat. No.:E-AB-93051, Houston, TX, USA). Additionally, recombinant anti-tau (phospho T231) antibody (abcam, Cat. No.: ab151559, Cambridge, UK) was used to determine the presence of Ptau in the brain sections. The amount of NF-κB and Ptau were determined by calculating the average area percent expression of randomly selected fields in each region.

4.7. Determination of Mitochondrial Membrane Potential

Mitochondrial membrane potential (MMP) was determined directly in the tissue by using image-iT™ TMRM reagent (Thermo Fisher Scientific, Waltham, MA, USA). TMRM is a cell-permeant dye that is taken by the active mitochondria and emits a fluorescence signals. Briefly, the tissue has been fixed on a microscopical slide and mixed with 10 µL of the staining solution and followed by incubation for 30 min at 37 °C in dark. The fluorescence signals were detected with the green filter of FLoid™ Cell Imaging Station (Thermo Fisher Scientific, Waltham, MA, USA). Fluorescence intensity was evaluated by ImageJ software (version 1.53K) to calculate corrected total cell fluorescence (CTCF) using the equation: [(integrated density − (area of selected cell × mean fluorescence of background readings)] [53].

4.8. Determination of Inflammatory Cytokines

The serum levels of tumor necrosis factor-alpha (TNF-α; Cat. No. E-EL-M3063) and interleukin-6 (IL-6; Cat. No. E-EL-M0044) were determined by using commercial ELISA kits supplied from Elabscience® (Houston, TX, USA) according to the supplier's instructions. Briefly, a volume of 100 µL of sample was introduced to the 96- well plate and subjected to incubation for 1 h at 37 °C. After that, 100 µL of biotinylated detection Ab working Solution and HRP conjugate working solution were added, followed by incubation at 37 °C for 1 h and 30 min, respectively. After the introduction of substrate solution and stop solution, the absorbance was taken at 450 nm for both TNF-α and IL-6.

4.9. Determination of IκB-α and IKK-α

IκB-α (MyBioSource, San Diego, CA, USA, Cat. No: MBS3806541) and IKK-α (MyBioSource, San Diego, CA, USA, Cat. No: MBS728866) were determined by using commercial ELISA kits according to the manufacturer's instructions. Briefly, a total volume of 50 µL of standards and samples was added to a 96-well plate. This was followed by the addition of 100 µL HRP-conjugate and allowed for incubation at 37 °C for 1 h. After the introduction of substrate solution and stop solution, the absorbance was taken at 450 nm for both proteins.

4.10. Determination of PPAR-γ, NF-κB, BACE-1, Synapsin-2, and miR-9

PPAR-γ, NF-κB, BACE-1, synapsin-2, and miR-9 gene expression was determined using qRT-PCR. Total RNAs were isolated from the brain tissue homogenate using a RNeasy Mini Kit (Qiagen, Hilden, Germany). Then, the extracted RNAs were reverse transcribed into cDNAs by using EasyScript® First-Strand cDNA Synthesis SuperMix (TransGen Biotech Co., Ltd., Beijing, China). After that, the cDNAs were amplified with QuantiNova SYBR Green PCR Kit (Qiagen, Hilden, Germany). Samples were normalized to the expression of β-actin housekeeping gene. The primer sequences used are expressed in Table 2.

Table 2. Sequence of the used primers.

Gene	Forward	Reverse
PPAR-γ	ATCAGGTTTGGGCGGGATCG	GTCAAGATCGCCCTCGCCTT
NF-κB	TCTCGACCTCCACCGGATCT	GCCCGCCTAAGGTGAAGAGA
BACE-1	GGGAGCTGGGAGCTGGATTA	CCCAGCTACATCTGGACGC
Synapsin-2	GTGTGGTCTTCCAGGACCTGAT	GCTGTCGGATGAGCACAAAGTC
β-actin	GCTCCTCCTGAGCGCAAGTA	GCAGCTCAGTAACAGTCCGC

PPAR-γ: peroxisome proliferator-activated receptor gamma, NF-κB: nuclear factor kappa B, BACE-1: β-site amyloid precursor protein cleaving enzyme.

For the expression of miR-9, miRNA was isolated from brain tissue homogenate using miRNeasy® Micro Kit followed by using miRCURY LNA RT Kit and miRCURY LNA SYBR® Green PCR Kit for reverse transcription and amplification steps, respectively. The

SNORD68 housekeeping was used as a reference control. All Kits used for detection of miR-9 were supplied from Qiagen (Hilden, Germany). The results were expressed as relative quantification ($RQ = 2^{-\Delta\Delta Ct}$) to the normal control.

4.11. Determination of Amyloid Beta

The brain content of Aβ (1–42) was determined by using commercial ELISA kits supplied from Elabscience® (Houston, TX, USA, Cat. No. E-EL-M3010) according to the supplier's instructions as described for the inflammatory cytokines.

4.12. Determination of Phosphorylated Tau Protein (Ptau)

The brain content of Ptau was determined by immunohistochemistry by using recombinant anti-tau (phospho T231) antibody (abcam, Cat. No.: ab151559, Cambridge, UK).

4.13. Statistical Analysis

Data were analyzed via one-way analysis of variance (ANOVA) followed by Tukey as a post hoc test using SPSS software (Version 22.0). GraphPad Prism software (version 6.01) was used for figures. In all analyses, a p value of <0.05 was considered statistically significant.

5. Conclusions

The present study revealed that TQ has a positive impact on cognitive dysfunction and behavioral performance in SCOP-induced neurotoxicity. This is achieved through reactivation of the downregulated PPAR-γ signaling pathway, which linked to NF-κB inflammatory cascade. This modulation involved upregulation of miR-9 concomitantly with restoration of the MMP and decreasing the inflammatory mediators. This multilevel of neuronal protection has decreased the deposited amyloid plaques. The potential effectiveness of TQ offers a promising avenue as a protective agent against AD, contingent upon the upregulation of miR-9, which is linked to the inhibition of NF-κB and activation of PPAR-γ.

Author Contributions: Conceptualization, H.E.A.M. and A.I.E.; methodology, H.E.A.M., A.I.E., M.E.-S.G. and E.M.M.; software, M.S.A. and E.I.E.-B.; validation, M.E.-S.G. and M.A.S.; formal analysis, M.S.A. and E.I.E.-B.; investigation, H.E.A.M., A.I.E., M.E.-S.G. and E.M.M.; resources, M.S.A., E.I.E.-B. and M.A.S.; data curation, M.S.A., E.I.E.-B. and M.A.S.; writing—original draft preparation, M.E.-S.G. and E.M.M.; writing—review and editing, H.E.A.M. and A.I.E.; visualization, W.A.S. and A.A.A.; supervision, H.E.A.M., A.I.E. and E.M.M.; project administration, H.E.A.M., A.I.E. and E.M.M.; funding acquisition, W.A.S. and A.A.A. All authors have read and agreed to the published version of the manuscript.

Funding: This research received no external funding.

Institutional Review Board Statement: The study protocol was approved by the Research Ethical Committee (Faculty of Science, Menoufia University, Egypt, FGE123) and it complies with the Guide for the Care and Use of Laboratory Animals (National Research Council).

Informed Consent Statement: Not applicable.

Data Availability Statement: The data are available upon request from the corresponding author.

Conflicts of Interest: The authors declare no conflict of interest.

Sample Availability: Not applicable.

References

1. Selkoe, D.J. Soluble Oligomers of the Amyloid β-Protein: Impair Synaptic Plasticity and Behavior. In *Synaptic Plasticity and the Mechanism of Alzheimer's Disease*; Springer: Berlin/Heidelberg, Germany, 2008; Volume 192, pp. 89–102.
2. Brookmeyer, R.; Johnson, E.; Ziegler-Graham, K.; Arrighi, H.M. Forecasting the Global Burden of Alzheimer's Disease. *Alzheimer's Dement.* **2007**, *3*, 186–191. [CrossRef]
3. Mat Nuri, T.H.; Hong, Y.H.; Ming, L.C.; Mohd Joffry, S.; Othman, M.F.; Neoh, C.F. Knowledge on Alzheimer's Disease among Public Hospitals and Health Clinics Pharmacists in the State of Selangor, Malaysia. *Front. Pharmacol.* **2017**, *8*, 739. [CrossRef]

4. Ballard, C.; Gauthier, S.; Corbett, A.; Brayne, C.; Aarsland, D.; Jones, E. Alzheimer's Disease. *Lancet* **2011**, *377*, 1019–1031. [CrossRef]
5. Singh, R.K. Recent Trends in the Management of Alzheimer's Disease: Current Therapeutic Options and Drug Repurposing Approaches. *Curr. Neuropharmacol.* **2020**, *18*, 868–882. [CrossRef]
6. Imran, M.; Al Kury, L.T.; Nadeem, H.; Shah, F.A.; Abbas, M.; Naz, S.; Khan, A.; Li, S. Benzimidazole Containing Acetamide Derivatives Attenuate Neuroinflammation and Oxidative Stress in Ethanol-Induced Neurodegeneration. *Biomolecules* **2020**, *10*, 108. [CrossRef]
7. Rockwood, K. Biomarkers to Measure Treatment Effects in Alzheimer's Disease: What Should We Look For? *Int. J. Alzheimer's Dis.* **2011**, *2011*, 598175. [CrossRef] [PubMed]
8. Liu, P.-P.; Xie, Y.; Meng, X.-Y.; Kang, J.-S. History and Progress of Hypotheses and Clinical Trials for Alzheimer's Disease. *Signal Transduct. Target. Ther.* **2019**, *4*, 29. [CrossRef] [PubMed]
9. Riedel, G.; Bergman, J.; Vanderschuren, L.; Ellenbroek, B.; Willner, P. The Behavioural Pharmacology of Dementia. *Behav. Pharmacol.* **2017**, *28*, 91–93.
10. Silman, I.; Sussman, J.L. Acetylcholinesterase: 'Classical' and 'Non-Classical' Functions and Pharmacology. *Curr. Opin. Pharmacol.* **2005**, *5*, 293–302. [CrossRef] [PubMed]
11. Wang, M.; Qin, L.; Tang, B. MicroRNAs in Alzheimer's Disease. *Front. Genet.* **2019**, *10*, 153. [CrossRef]
12. Hébert, S.S.; Horré, K.; Nicolaï, L.; Papadopoulou, A.S.; Mandemakers, W.; Silahtaroglu, A.N.; Kauppinen, S.; Delacourte, A.; De Strooper, B. Loss of MicroRNA Cluster MiR-29a/b-1 in Sporadic Alzheimer's Disease Correlates with Increased BACE1/β-Secretase Expression. *Proc. Natl. Acad. Sci. USA* **2008**, *105*, 6415–6420. [CrossRef] [PubMed]
13. Müller, M.; Jäkel, L.; Bruinsma, I.B.; Claassen, J.A.; Kuiperij, H.B.; Verbeek, M.M. MicroRNA-29a Is a Candidate Biomarker for Alzheimer's Disease in Cell-Free Cerebrospinal Fluid. *Mol. Neurobiol.* **2016**, *53*, 2894–2899. [CrossRef] [PubMed]
14. Souza, V.C.; Morais, G.S., Jr.; Henriques, A.D.; Machado-Silva, W.; Perez, D.I.V.; Brito, C.J.; Camargos, E.F.; Moraes, C.F.; Nóbrega, O.T. Whole-Blood Levels of MicroRNA-9 Are Decreased in Patients with Late-Onset Alzheimer Disease. *Am. J. Alzheimer's Dis. Other Dement.* **2020**, *35*. [CrossRef] [PubMed]
15. Schonrock, N.; Ke, Y.D.; Humphreys, D.; Staufenbiel, M.; Ittner, L.M.; Preiss, T.; Götz, J. Neuronal MicroRNA Deregulation in Response to Alzheimer's Disease Amyloid-β. *PLoS ONE* **2010**, *5*, e11070. [CrossRef]
16. Schonrock, N.; Humphreys, D.T.; Preiss, T.; Götz, J. Target Gene Repression Mediated by MiRNAs MiR-181c and MiR-9 Both of Which Are down-Regulated by Amyloid-β. *J. Mol. Neurosci.* **2012**, *46*, 324–335. [CrossRef]
17. Che, H.; Sun, L.-H.; Guo, F.; Niu, H.-F.; Su, X.-L.; Bao, Y.-N.; Fu, Z.D.; Liu, H.; Hou, X.; Yang, B.-F. Expression of Amyloid-Associated MiRNAs in Both the Forebrain Cortex and Hippocampus of Middle-Aged Rat. *Cell. Physiol. Biochem.* **2014**, *33*, 11–22. [CrossRef]
18. Chang, F.; Zhang, L.; Xu, W.; Jing, P.; Zhan, P. MicroRNA-9 Attenuates Amyloidβ-induced Synaptotoxicity by Targeting Calcium/Calmodulin-Dependent Protein Kinase Kinase 2. *Mol. Med. Rep.* **2014**, *9*, 1917–1922. [CrossRef]
19. Snow, W.M.; Albensi, B.C. Neuronal Gene Targets of NF-KB and Their Dysregulation in Alzheimer's Disease. *Front. Mol. Neurosci.* **2016**, *9*, 118. [CrossRef]
20. Jones, S.V.; Kounatidis, I. Nuclear Factor-Kappa B and Alzheimer Disease, Unifying Genetic and Environmental Risk Factors from Cell to Humans. *Front. Immunol.* **2017**, *8*, 1805. [CrossRef]
21. Oeckinghaus, A.; Ghosh, S. The NF-KappaB Family of Transcription Factors and Its Regulation. *Cold Spring Harb. Perspect. Biol.* **2009**, *1*, a000034. [CrossRef]
22. Liu, T.; Zhang, L.; Joo, D.; Sun, S.C. NF-KB Signaling in Inflammation. *Signal Transduct. Target. Ther.* **2017**, *2*, 17023. [CrossRef]
23. Bronzuoli, M.R.; Iacomino, A.; Steardo, L.; Scuderi, C. Targeting Neuroinflammation in Alzheimer's Disease. *J. Inflamm. Res.* **2016**, *9*, 199–208. [CrossRef] [PubMed]
24. Agarwal, S.; Yadav, A.; Chaturvedi, R.K. Peroxisome Proliferator-Activated Receptors (PPARs) as Therapeutic Target in Neurodegenerative Disorders. *Biochem. Biophys. Res. Commun.* **2017**, *483*, 1166–1177. [CrossRef] [PubMed]
25. Gad, D.; Mansour, H.E.A.; Saad-Allah, K.M.; Abdallah, M.S.; Elberri, A.I.; Mosalam, E.M. Biostimulants Improve the Hepatoprotection of Ammi Visnaga Seed Yield Extract against Carbon Tetrachloride Induced Acute Hepatitis in Mice through Modulation of MAPK. *Saudi J. Biol. Sci.* **2022**. [CrossRef]
26. Abo Mansour, H.E.; El-Batsh, M.M.; Badawy, N.S.; Mehanna, E.T.; Mesbah, N.M.; Abo-Elmatty, D.M. Ginger Extract Loaded into Chitosan Nanoparticles Enhances Cytotoxicity and Reduces Cardiotoxicity of Doxorubicin in Hepatocellular Carcinoma in Mice. *Nutr. Cancer* **2021**, *73*, 2347–2362. [CrossRef]
27. El-Ashmawy, N.E.; Khedr, N.F.; El-Bahrawy, H.A.; Abo Mansour, H.E. Ginger Extract Adjuvant to Doxorubicin in Mammary Carcinoma: Study of Some Molecular Mechanisms. *Eur. J. Nutr.* **2018**, *57*, 981–989. [CrossRef]
28. Mosalam, E.M.; Zidan, A.-A.A.; Mehanna, E.T.; Mesbah, N.M.; Abo-Elmatty, D.M. Thymoquinone and Pentoxifylline Enhance the Chemotherapeutic Effect of Cisplatin by Targeting Notch Signaling Pathway in Mice. *Life Sci.* **2020**, *244*, 117299. [CrossRef]
29. Zidan, A.-A.A.; El-Ashmawy, N.E.; Khedr, E.G.; Ebeid, E.-Z.M.; Salem, M.L.; Mosalam, E.M. Loading of Doxorubicin and Thymoquinone with F2 Gel Nanofibers Improves the Antitumor Activity and Ameliorates Doxorubicin-Associated Nephrotoxicity. *Life Sci.* **2018**, *207*, 461–470. [CrossRef]
30. Alhebshi, A.H.; Gotoh, M.; Suzuki, I. Thymoquinone Protects Cultured Rat Primary Neurons against Amyloid β-Induced Neurotoxicity. *Biochem. Biophys. Res. Commun.* **2013**, *433*, 362–367. [CrossRef]

31. Bargi, R.; Asgharzadeh, F.; Beheshti, F.; Hosseini, M.; Sadeghnia, H.R.; Khazaei, M. The Effects of Thymoquinone on Hippocampal Cytokine Level, Brain Oxidative Stress Status and Memory Deficits Induced by Lipopolysaccharide in Rats. *Cytokine* **2017**, *96*, 173–184. [CrossRef]
32. Beker, M.; Dallı, T.; Elibol, B. Thymoquinone Can Improve Neuronal Survival and Promote Neurogenesis in Rat Hippocampal Neurons. *Mol. Nutr. Food Res.* **2018**, *62*, 1700768. [CrossRef] [PubMed]
33. Oh, J.H.; Choi, B.J.; Chang, M.S.; Park, S.K. Nelumbo Nucifera Semen Extract Improves Memory in Rats with Scopolamine-Induced Amnesia through the Induction of Choline Acetyltransferase Expression. *Neurosci. Lett.* **2009**, *461*, 41–44. [CrossRef] [PubMed]
34. Chopin, P.; Briley, M. Effects of Four Non-Cholinergic Cognitive Enhancers in Comparison with Tacrine and Galanthamine on Scopolamine-Induced Amnesia in Rats. *Psychopharmacology* **1992**, *106*, 26–30. [CrossRef] [PubMed]
35. Kazmi, I.; Al-Abbasi, F.A.; Afzal, M.; Nadeem, M.S.; Altayb, H.N. Sterubin Protects against Chemically-Induced Alzheimer's Disease by Reducing Biomarkers of Inflammation-IL-6/IL-β/TNF-α and Oxidative Stress-SOD/MDA in Rats. *Saudi J. Biol. Sci.* **2023**, *30*, 103560. [CrossRef]
36. AlGhamdi, S.A.; Al-Abbasi, F.A.; Alghamdi, A.M.; Omer, A.B.; Afzal, O.; Altamimi, A.S.A.; Alamri, A.; Alzarea, S.I.; Almalki, W.H.; Kazmi, I. Barbigerone Prevents Scopolamine-Induced Memory Impairment in Rats by Inhibiting Oxidative Stress and Acetylcholinesterase Levels. *R. Soc. Open Sci.* **2023**, *10*, 230013. [CrossRef]
37. Poorgholam, P.; Yaghmaei, P.; Hajebrahimi, Z. Thymoquinone Recovers Learning Function in a Rat Model of Alzheimer's Disease. *Avicenna J. Phytomed.* **2018**, *8*, 188–197.
38. He, Z.; Han, S.; Wu, C.; Liu, L.; Zhu, H.; Liu, A.; Lu, Q.; Huang, J.; Du, X.; Li, N. Bis (Ethylmaltolato) Oxidovanadium (Iv) Inhibited the Pathogenesis of Alzheimer's Disease in Triple Transgenic Model Mice. *Metallomics* **2020**, *12*, 474–490. [CrossRef]
39. Yuliana, A.; Daijo, A.; Jheng, H.-F.; Kwon, J.; Nomura, W.; Takahashi, H.; Ara, T.; Kawada, T.; Goto, T. Endoplasmic Reticulum Stress Impaired Uncoupling Protein 1 Expression via the Suppression of Peroxisome Proliferator-Activated Receptor γ Binding Activity in Mice Beige Adipocytes. *Int. J. Mol. Sci.* **2019**, *20*, 274. [CrossRef]
40. Ricote, M.; Li, A.C.; Willson, T.M.; Kelly, C.J.; Glass, C.K. The Peroxisome Proliferator-Activated Receptor-γ Is a Negative Regulator of Macrophage Activation. *Nature* **1998**, *391*, 79–82. [CrossRef]
41. Majdalawieh, A.; Ro, H.-S. PPARγ1 and LXRα Face a New Regulator of Macrophage Cholesterol Homeostasis and Inflammatory Responsiveness, AEBP1. *Nucl. Recept. Signal.* **2010**, *8*, nrs-08004. [CrossRef]
42. Dehmer, T.; Heneka, M.T.; Sastre, M.; Dichgans, J.; Schulz, J.B. Protection by Pioglitazone in the MPTP Model of Parkinson's Disease Correlates with IκBα Induction and Block of NFκB and INOS Activation. *J. Neurochem.* **2004**, *88*, 494–501. [CrossRef] [PubMed]
43. Quan, Q.; Qian, Y.; Li, X.; Li, M. Pioglitazone Reduces β Amyloid Levels via Inhibition of PPARγ Phosphorylation in a Neuronal Model of Alzheimer's Disease. *Front. Aging Neurosci.* **2019**, *11*, 178. [CrossRef]
44. Xiang, G.Q.; Tang, S.S.; Jiang, L.Y.; Hong, H.; Li, Q.; Wang, C.; Wang, X.Y.; Zhang, T.T.; Yin, L. PPAR γ Agonist Pioglitazone Improves Scopolamine-Induced Memory Impairment in Mice. *J. Pharm. Pharmacol.* **2012**, *64*, 589–596. [CrossRef] [PubMed]
45. Reich, D.; Gallucci, G.; Tong, M.; de la Monte, S.M. Therapeutic Advantages of Dual Targeting of PPAR-δ and PPAR-γ in an Experimental Model of Sporadic Alzheimer's Disease. *J. Park. Dis. Alzheimer's Dis.* **2018**, *5*. [CrossRef]
46. Chen, Y.; Wang, B.; Zhao, H. Thymoquinone Reduces Spinal Cord Injury by Inhibiting Inflammatory Response, Oxidative Stress and Apoptosis via PPAR-γ and PI3K/Akt Pathways. *Exp. Ther. Med.* **2018**, *15*, 4987–4994. [CrossRef]
47. Hussien, N.I.; Elawady, M.A.; Elmaghrabi, M.M.; Muhammad, M.H. Impact of Thymoquinone on Memory Deficit-Associated with Global Cerebral Ischemia-Reperfusion Injury in Rats; Possible Role of PPAR-γ. *Am. J. Biomed. Sci.* **2020**, *12*, 77–90. [CrossRef]
48. Zaher, M.; Bendary, M.; El-Aziz, G.; Ali, A. Potential Protective Role of Thymoquinone on Experimentally-induced Alzheimer Rats. *J. Pharm. Res. Int.* **2019**, *31*, 1–18. [CrossRef]
49. Prescott, J.A.; Mitchell, J.P.; Cook, S.J. Inhibitory Feedback Control of NF-KB Signalling in Health and Disease. *Biochem. J.* **2021**, *478*, 2619–2664. [CrossRef]
50. Cobourne-Duval, M.K.; Taka, E.; Mendonca, P.; Bauer, D.; Soliman, K.F.A. The Antioxidant Effects of Thymoquinone in Activated BV-2 Murine Microglial Cells. *Neurochem. Res.* **2016**, *41*, 3227–3238. [CrossRef]
51. Abulfadl, Y.S.; El-Maraghy, N.N.; Ahmed, A.A.E.; Nofal, S.; Abdel-Mottaleb, Y.; Badary, O.A. Thymoquinone Alleviates the Experimentally Induced Alzheimer's Disease Inflammation by Modulation of TLRs Signaling. *Hum. Exp. Toxicol.* **2018**, *37*, 1092–1104. [CrossRef]
52. Thummuri, D.; Jeengar, M.K.; Shrivastava, S.; Nemani, H.; Ramavat, R.N.; Chaudhari, P.; Naidu, V.G.M. Thymoquinone Prevents RANKL-Induced Osteoclastogenesis Activation and Osteolysis in an in Vivo Model of Inflammation by Suppressing NF-KB and MAPK Signalling. *Pharmacol. Res.* **2015**, *99*, 63–73. [CrossRef] [PubMed]
53. Mosalam, E.M.; Elberri, A.I.; Sallam, A.S.; Salem, H.R.; Metwally, E.M.; Abdallah, M.S.; Shaldam, M.A.; Mansour, H.E.A. Chronotherapeutic Neuroprotective Effect of Verapamil against Lipopolysaccharide-Induced Neuroinflammation in Mice through Modulation of Calcium-Dependent Genes. *Mol. Med.* **2022**, *28*, 139. [CrossRef] [PubMed]
54. Swerdlow, R.H. Mitochondria and Mitochondrial Cascades in Alzheimer's Disease. *J. Alzheimer's Dis.* **2018**, *62*, 1403–1416. [CrossRef] [PubMed]
55. Eckert, A.; Schmitt, K.; Götz, J. Mitochondrial Dysfunction-the Beginning of the End in Alzheimer's Disease? Separate and Synergistic Modes of Tau and Amyloid-β Toxicity. *Alzheimer's Res. Ther.* **2011**, *3*, 15. [CrossRef]

56. Corona, J.C.; Duchen, M.R. PPARγ as a Therapeutic Target to Rescue Mitochondrial Function in Neurological Disease. *Free Radic. Biol. Med.* **2016**, *100*, 153–163. [CrossRef]
57. Fan, Y.; Hu, J.; Li, J.; Yang, Z.; Xin, X.; Wang, J.; Ding, J.; Geng, M. Effect of Acidic Oligosaccharide Sugar Chain on Scopolamine-Induced Memory Impairment in Rats and Its Related Mechanisms. *Neurosci. Lett.* **2005**, *374*, 222–226. [CrossRef]
58. El-Sherbiny, D.A.; Khalifa, A.E.; Attia, A.S.; Eldenshary, E.E.-D.S. Hypericum Perforatum Extract Demonstrates Antioxidant Properties against Elevated Rat Brain Oxidative Status Induced by Amnestic Dose of Scopolamine. *Pharmacol. Biochem. Behav.* **2003**, *76*, 525–533. [CrossRef]
59. Jeong, E.J.; Lee, K.Y.; Kim, S.H.; Sung, S.H.; Kim, Y.C. Cognitive-Enhancing and Antioxidant Activities of Iridoid Glycosides from Scrophularia Buergeriana in Scopolamine-Treated Mice. *Eur. J. Pharmacol.* **2008**, *588*, 78–84. [CrossRef]
60. Ismail, N.; Ismail, M.; Mazlan, M.; Latiff, L.A.; Imam, M.U.; Iqbal, S.; Azmi, N.H.; Ghafar, S.A.A.; Chan, K.W. Thymoquinone Prevents β-Amyloid Neurotoxicity in Primary Cultured Cerebellar Granule Neurons. *Cell. Mol. Neurobiol.* **2013**, *33*, 1159–1169. [CrossRef]
61. Qian, D.; Wei, G.; Xu, C.; He, Z.; Hua, J.; Li, J.; Hu, Q.; Lin, S.; Gong, J.; Meng, H. Bone Marrow-Derived Mesenchymal Stem Cells (BMSCs) Repair Acute Necrotized Pancreatitis by Secreting MicroRNA-9 to Target the NF-KB1/P50 Gene in Rats. *Sci. Rep.* **2017**, *7*, 581. [CrossRef]
62. Lee, W.S.; Yasuda, S.; Kono, M.; Kudo, Y.; Shimamura, S.; Kono, M.; Fujieda, Y.; Kato, M.; Oku, K.; Shimizu, T. MicroRNA-9 Ameliorates Destructive Arthritis through down-Regulation of NF-KB1-RANKL Pathway in Fibroblast-like Synoviocytes. *Clin. Immunol.* **2020**, *212*, 108348. [CrossRef] [PubMed]
63. Gu, R.; Liu, N.; Luo, S.; Huang, W.; Zha, Z.; Yang, J. MicroRNA-9 Regulates the Development of Knee Osteoarthritis through the NF-KappaB1 Pathway in Chondrocytes. *Medicine* **2016**, *95*, e4315. [CrossRef] [PubMed]
64. Giusti, S.A.; Vogl, A.M.; Brockmann, M.M.; Vercelli, C.A.; Rein, M.L.; Trümbach, D.; Wurst, W.; Cazalla, D.; Stein, V.; Deussing, J.M. MicroRNA-9 Controls Dendritic Development by Targeting REST. *eLife* **2014**, *3*, e02755. [CrossRef] [PubMed]
65. Yao, H.; Ma, R.; Yang, L.; Hu, G.; Chen, X.; Duan, M.; Kook, Y.; Niu, F.; Liao, K.; Fu, M. MiR-9 Promotes Microglial Activation by Targeting MCPIP1. *Nat. Commun.* **2014**, *5*, 4386. [CrossRef] [PubMed]
66. Li, S.-H.; Gao, P.; Wang, L.-T.; Yan, Y.-H.; Xia, Y.; Song, J.; Li, H.-Y.; Yang, J.-X. Osthole Stimulated Neural Stem Cells Differentiation into Neurons in an Alzheimer's Disease Cell Model via Upregulation of MicroRNA-9 and Rescued the Functional Impairment of Hippocampal Neurons in APP/PS1 Transgenic Mice. *Front. Neurosci.* **2017**, *11*, 340. [CrossRef] [PubMed]
67. Praticò, D. The Functional Role of MicroRNAs in the Pathogenesis of Tauopathy. *Cells* **2020**, *9*, 2262. [CrossRef]
68. Hitt, B.; Riordan, S.M.; Kukreja, L.; Eimer, W.A.; Rajapaksha, T.W.; Vassar, R. β-Site Amyloid Precursor Protein (APP)-Cleaving Enzyme 1 (BACE1)-Deficient Mice Exhibit a Close Homolog of L1 (CHL1) Loss-of-Function Phenotype Involving Axon Guidance Defects. *J. Biol. Chem.* **2012**, *287*, 38408–38425. [CrossRef]
69. Peters, F.; Salihoglu, H.; Rodrigues, E.; Herzog, E.; Blume, T.; Filser, S.; Dorostkar, M.; Shimshek, D.R.; Brose, N.; Neumann, U. BACE1 Inhibition More Effectively Suppresses Initiation than Progression of β-Amyloid Pathology. *Acta Neuropathol.* **2018**, *135*, 695–710. [CrossRef]
70. Cao, G.; Su, P.; Zhang, S.; Guo, L.; Zhang, H.; Liang, Y.; Qin, C.; Zhang, W. Ginsenoside Re Reduces Aβ Production by Activating PPARγ to Inhibit BACE1 in N2a/APP695 Cells. *Eur. J. Pharmacol.* **2016**, *793*, 101–108. [CrossRef]
71. Lin, N.; Chen, L.; Pan, X.; Zhu, Y.; Zhang, J.; Shi, Y.; Chen, X. Tripchlorolide Attenuates β-Amyloid Generation via Suppressing PPARγ-Regulated BACE1 Activity in N2a/APP695 Cells. *Mol. Neurobiol.* **2016**, *53*, 6397–6406. [CrossRef]
72. Jahan, R.; Yousaf, M.; Khan, H.; Shah, S.A.; Khan, A.A.; Bibi, N.; Javed, F.; Ijaz, M.; Ali, A.; Wei, D.-Q. Zinc Ortho Methyl Carbonodithioate Improved Pre and Post-Synapse Memory Impairment via SIRT1/p-JNK Pathway against Scopolamine in Adult Mice. *J. Neuroimmune Pharmacol.* **2023**, *18*, 183–194. [CrossRef] [PubMed]
73. Elibol, B.; Beker, M.; Terzioglu-Usak, S.; Dalli, T.; Kilic, U. Thymoquinone Administration Ameliorates Alzheimer's Disease-like Phenotype by Promoting Cell Survival in the Hippocampus of Amyloid Beta1–42 Infused Rat Model. *Phytomedicine* **2020**, *79*, 153324. [CrossRef] [PubMed]
74. Ismail, N.; Ismail, M.; Azmi, N.H.; Bakar, M.F.A.; Yida, Z.; Abdullah, M.A.; Basri, H. Thymoquinone-Rich Fraction Nanoemulsion (TQRFNE) Decreases Aβ40 and Aβ42 Levels by Modulating APP Processing, up-Regulating IDE and LRP1, and down-Regulating BACE1 and RAGE in Response to High Fat/Cholesterol Diet-Induced Rats. *Biomed. Pharmacother.* **2017**, *95*, 780–788. [CrossRef] [PubMed]
75. Corradi, A.; Zanardi, A.; Giacomini, C.; Onofri, F.; Valtorta, F.; Zoli, M.; Benfenati, F. Synapsin-I-and Synapsin-II-Null Mice Display an Increased Age-Dependent Cognitive Impairment. *J. Cell Sci.* **2008**, *121*, 3042–3051. [CrossRef] [PubMed]
76. Lukiw, W.J. NF-κB-Regulated Micro RNAs (MiRNAs) in Primary Human Brain Cells. *Exp. Neurol.* **2012**, *235*, 484–490. [CrossRef]
77. Chiang, M.-C.; Cheng, Y.-C.; Chen, H.-M.; Liang, Y.-J.; Yen, C.-H. Rosiglitazone Promotes Neurite Outgrowth and Mitochondrial Function in N2A Cells via PPARgamma Pathway. *Mitochondrion* **2014**, *14*, 7–17. [CrossRef]
78. Zhang, G.; Zheng, D.; Yu, H.; Luo, X.; Wu, W. Ginkgo Biloba Extract Ameliorates Scopolamine-Induced Memory Deficits via Rescuing Synaptic Damage. *Curr. Med. Sci.* **2022**, *42*, 474–482. [CrossRef]
79. Nie, L.; Xia, J.; Li, H.; Zhang, Z.; Yang, Y.; Huang, X.; He, Z.; Liu, J.; Yang, X. Ginsenoside Rg1 Ameliorates Behavioral Abnormalities and Modulates the Hippocampal Proteomic Change in Triple Transgenic Mice of Alzheimer's Disease. *Oxid. Med. Cell. Longev.* **2017**, *2017*, 6473506. [CrossRef]

80. Kwon, S.-H.; Kim, H.-C.; Lee, S.-Y.; Jang, C.-G. Loganin Improves Learning and Memory Impairments Induced by Scopolamine in Mice. *Eur. J. Pharmacol.* **2009**, *619*, 44–49. [CrossRef]
81. Alobaedi, O.H.; Talib, W.H.; Basheti, I.A. Antitumor Effect of Thymoquinone Combined with Resveratrol on Mice Transplanted with Breast Cancer. *Asian Pac. J. Trop. Med.* **2017**, *10*, 400–408. [CrossRef]
82. DeTure, M.A.; Dickson, D.W. The Neuropathological Diagnosis of Alzheimer's Disease. *Mol. Neurodegener.* **2019**, *14*, 32. [CrossRef] [PubMed]